PLOS ONE

RESEARCH ARTICLE

Crop loss identification at field parcel scale using satellite remote sensing and machine learning

Santosh Hiremath[1☯*], **Samantha Wittke**[2,3☯], **Taru Palosuo**[4], **Jere Kaivosoja**[4], **Fulu Tao**[4], **Maximilian Proll**[1], **Eetu Puttonen**[2], **Pirjo Peltonen-Sainio**[4‡], **Pekka Marttinen**[1‡], **Hiroshi Mamitsuka**[1,5‡]

1 Department of Computer Science, Aalto University, Espoo, Finland, **2** Finnish Geospatial Research Institute, Masala, Finland, **3** Department of Built Environment, Aalto University, Espoo, Finland, **4** Natural Resources Institute Finland (Luke), Helsinki, Finland, **5** Bioinformatics Center, Institute for Chemical Research, Kyoto University, Uji, Japan

☯ These authors contributed equally to this work.
‡ These authors also contributed equally to this work.
* santosh.hiremath@aalto.fi

Citation: Hiremath S, Wittke S, Palosuo T, Kaivosoja J, Tao F, Proll M, et al. (2021) Crop loss identification at field parcel scale using satellite remote sensing and machine learning. PLoS ONE 16(12): e0251952. https://doi.org/10.1371/journal.pone.0251952

Editor: Gerald Forkuor, United Nations University Institute for Natural Resources in Africa, GHANA

Received: May 4, 2021

Accepted: November 26, 2021

Published: December 16, 2021

Data Availability Statement: There are legal restrictions on sharing the reference data used in this study that was provided by the Finnish Food Authority. This is because the reference data contains identifiable information about the field parcels (their boundaries, locations, etc.). Simply showing them on a map (without providing explicit coordinates) may lead to their identification. However, permission to access the data can be obtained from Finnish Food Authority at through email kirjaamo@foodauthority.fi, phone: +358 29 530 0400 or through the webiste: https://www.

Abstract

Identifying crop loss at field parcel scale using satellite images is challenging: first, crop loss is caused by many factors during the growing season; second, reliable reference data about crop loss are lacking; third, there are many ways to define crop loss. This study investigates the feasibility of using satellite images to train machine learning (ML) models to classify agricultural field parcels into those with and without crop loss. The reference data for this study was provided by Finnish Food Authority (FFA) containing crop loss information of approximately 1.4 million field parcels in Finland covering about 3.5 million ha from 2000 to 2015. This reference data was combined with Normalised Difference Vegetation Index (NDVI) derived from Landsat 7 images, in which more than 80% of the possible data are missing. Despite the hard problem with extremely noisy data, among the four ML models we tested, random forest (with mean imputation and missing value indicators) achieved the average AUC (area under the ROC curve) of 0.688±0.059 over all 16 years with the range [0.602, 0.795] in identifying new crop-loss fields based on reference fields of the same year. To our knowledge, this is one of the first large scale benchmark study of using machine learning for crop loss classification at field parcel scale. The classification setting and trained models have numerous potential applications, for example, allowing government agencies or insurance companies to verify crop-loss claims by farmers and realise efficient agricultural monitoring.

1 Introduction

Future food production is challenged by increasing demand for more sustainable agricultural systems that consider environmental, economic and social dimensions of sustainability.

ruokavirasto.fi/en/about-us/services/service-numbers/. With the exception of the reference data and the derived time series we can provide all other forms of data including the code, Landsat 7 scenes, and the trained models. 1. The code used to train and test the models is available at https://github.com/satnih/crop_loss_identification 2. Landsat 7 scenes used in the study can be downloaded from Earth Explorer (https://earthexplorer.usgs.gov/) with the code in the 'prepare data' folder in the above GitHub link. 3. The GitHub repository also contains a synthetic data set to help verify that the code executes successfully. Note that the synthetic data cannot be used to reproduce the results and tables in the manuscript. We hope that our above response meets the data usage criterion of PLOS. If you still have problems regarding this point, please do not hesitate to let us know so that we can reconsider this issue.

Funding: This joint research between Aalto University and Natural Resources Institute Finland (Luke) is funded by the AIPSE programme of Academy of Finland through the AI-CropPro project; decision number 315896 (Aalto) and 316172 (Luke).

Competing interests: The authors have declared that no competing interests exist.

Remote sensing data from spaceborne platforms offer a possibility to address these challenges [1]. Multispectral satellite remote sensing applications in agriculture date back to the early 1970s with the launch of Landsat 1 by the National Aeronautics and Space Agency (NASA). Applications include agriculture land use mapping [2], agricultural monitoring [3], leaf area index (LAI) and biomass estimation [4, 5], precision agriculture [6], agricultural water management [7], estimation of crop yield [8–13], and crop damage assessment caused by floods [14, 15] and lodging [16]. These studies have focused mostly on the regional scale due to a spatially limited reference data at a field parcel scale.

Only a few studies have considered the use of remote sensing data from spaceborne platforms to assess crop loss at field parcel scale. For example, multispectral spaceborne remote sensing data from Landsat ETM+ was used to study the effect of sowing date and weed control during fallow period on spring wheat yield in Mexico by [17]. Based on experiments on 100 fields across three seasons they concluded that the effect of sowing data and weed control on yield can be estimated using multispectral spaceborne remote sensing data. Tapia-Silva et al. [14] studied crop losses due to flood using Landsat TM/ETM on 132 field parcels across 15 seasons and concluded that modelling crop loss was challenging. Data from Sentinel-1 and 2 satellites were used by [18] for cyclone damage assessment on 200 coconut and 200 rice fields in India with promising results. Crop damages on 600 wheat fields were also studied by [19] in Greece using spaceborne multispectral imagery and ancillary geospatial data, but they faced the challenge of defining field parcels based on low resolution imagery available from spaceborne platforms. Two recent studies [20, 21] used Synthetic Aperture Radar (SAR) images to assess crop damage due the 2020 wind storm Derecho. They apply their method across the state of Iowa, United States to estimate the area of crop damage and verify their methods with ground truth data of a maximum of 14 fields. A common theme across many of the above studies is the limited number of ground truth data from field parcels used to evaluate the proposed methods. This is understandable because collecting large amounts of ground truth data from many field parcels is challenging. In summary, to the best of our knowledge, remote sensing applications have been limited to specific crop-loss type based on its cause such as flooding or drought and are also limited to coarse spatial scale due to lack of ground truth data. A large study about the use of remote sensing data for monitoring general crop loss (not specific to any causal factor) at field parcel scale is desirable. Because it can aid both public and private organisations like insurance companies and governments, respectively, in agricultural monitoring [22, 23]. Such a study can also aid in effective implementation of Common Agricultural Policy (CAP) reforms enacted by the European Commission (EC) [24]. In fact EC has started projects such as Sentinels for CAP (Sen4Cap), aimed at developing new remote sensing methods for agricultural monitoring at scale [25].

There are many drivers for crop loss. Yield potential in a given field and region depends on the crop and cultivar. In addition to a soil type and weather conditions, farmer's decisions have an impact on yield potential and the risk for crop loss. The risk of crop loss can be reduced by using quality seeds [26], planting well-adapted cultivars [27], matching crops to the most appropriate field parcels [28], as well as by adopting timely and accurate management practices such as sowing, crop protection and harvesting. For high-latitude agricultural systems risks caused by variable weather are substantial, and total large scale crop failures may occur once or twice a decade [29]. In this study, we use the definition of crop loss of Finnish crop damage compensation program. It is given by the percentage of area of field parcel. This definition decouples crop loss from its driver allowing the study of general crop loss irrespective of the driver.

This study aims to test the feasibility of combining machine learning (ML) models with optical satellite data to classify field parcels with and without crop loss. The reference data used

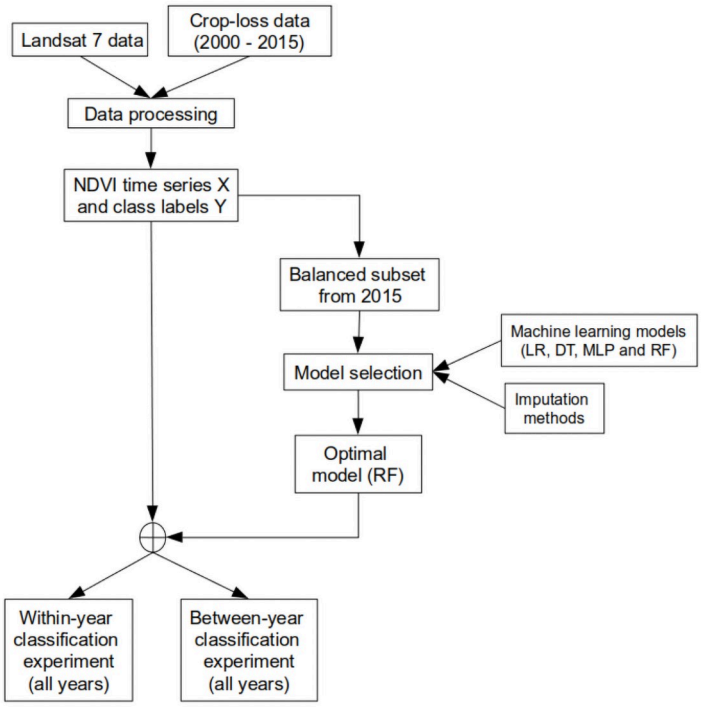

Fig 1. Overview of the study as a flowchart.

https://doi.org/10.1371/journal.pone.0251952.g001

consists of approximately 1.4 million barley (*Hordeum vulgare* L.) fields covering 3.5 million ha in Finland. The time period of the study is sixteen years from 2000 to 2015. Two settings are considered: 1) within-year classification, where training and test data are from the same year and 2) between-year classification, where training and test data are from different years. Both can be applied to the task of verifying a crop loss reported by a farmer, while 1) corresponds to the situation where data from other fields are available in the respective year, whereas in 2) no such data are available. The overview of the study is illustrated in the form of a flowchart in Fig 1. Performance results (AUC) obtained for within-year classification was approximately 0.7 on average over 16 years, while the regression line estimated by the projection of our results implied this performance can be improved if the missing data ratio was reduced. Analysis of the results revealed high amount of missing data in satellite image time series (more than 80% in our case) can have a significant impact on the classification performance. Thanks to the very comprehensive data set and wide spread of the area of investigation, we expect that our conclusions regarding the classification performance of the methods to be robust and generalisable for Barley in other countries.

2 Materials and methods

2.1 Study area and crop loss data

The study area includes southern and western regions of Finland from 2000 to 2015. The area investigated covers the coastal agricultural land area in Finland comprising of 1.4 million field parcels growing barley and covering approximately 3.5 million ha. The size of the field parcels varied from 1 to 90 ha with an average of 2.4 ha. The study area and the distribution of the field parcels are shown in Fig 2.

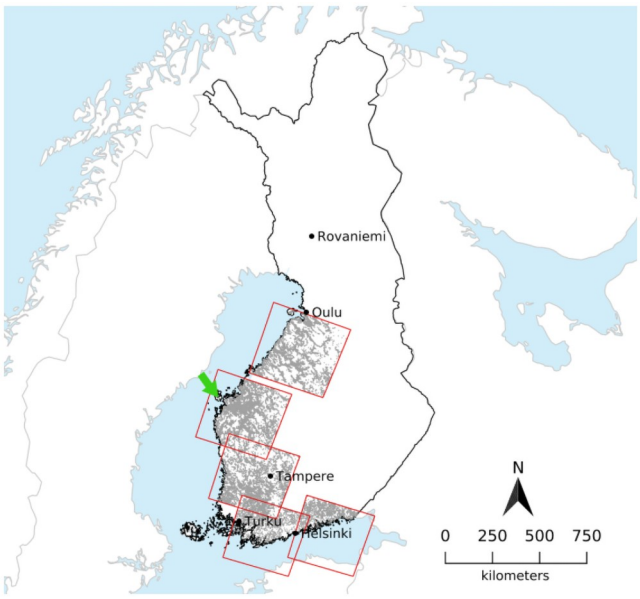

Fig 2. Study area. Landsat-7 tiles extent (red) over South-Western Finland utilised in this study with barley fields of the year 2000 added in grey. Centre coordinates (latitude, longitude) of the Landsat 7 tiles from North to South: 19015: 64.22478116, 25.13267424; 19116: 62.85736322, 22.45274870; 19017: 61.48156017, 22.95909640; 18918 (southwestern): 60.10043047, 23.54123385; 18718 (southeastern): 60.09748833, 26.63623269; background: Natural Earth, Finland: National Land Survey of Finland Topographic Database 05/2021. The green arrow denotes the location of the subset shown in Fig 3.

https://doi.org/10.1371/journal.pone.0251952.g002

The reference data on crop loss was provided by Finnish Food Authority (FFA). The data consisted of field parcel ID, field boundary (see example area in Fig 3), area, crop type and variety, crop loss (as area of the field parcel) and farm ID for the years from 2000 to 2015. The data originates from the crop damage compensation system in Finland that started in 1976 and lasted until 2015 [30]. The analysis was made with barley as it most amount of reference data among all the crops.

The crop loss data were collected through a self-reporting survey where the farmers reported crop loss as percentage of the area of the field. This was processed into a binary variable where anything greater than zero percent indicated crop loss (1) and everything else as indicated no loss (0). The number of field parcels with and without crop loss for each year from 2000 to 2015 is shown in Table 1. Over all years and the whole area of investigation, there were 33,840 field parcels (2.38%) with crop loss and 1,418,872 (97.62%) with no loss. We observed that larger fields had reported loss more often than smaller fields so the effect of field size on crop loss classification performance was examined (see the last part of Section 3.2).

The reference data also includes reasons for crop loss that were sporadically provided by the farmer. Fig 4 shows the numbers of barley fields affected by different drivers of crop losses. It can be seen that the main reasons for crop loss reported by farmers for barley in Finland were related to an over- or under-supply of water.

2.2 Satellite data

Landsat 7 ETM+ (Enhanced Thematic Mapper [31]) satellite data was chosen for the study to cover the area and time frame of the reference data. Landsat 7 was launched in April 1999 and is still operating as of May 2020. It carries a multispectral sensor, which provides 8 bands covering the visible range, near-infrared and mid-infrared range as well as one thermal infrared

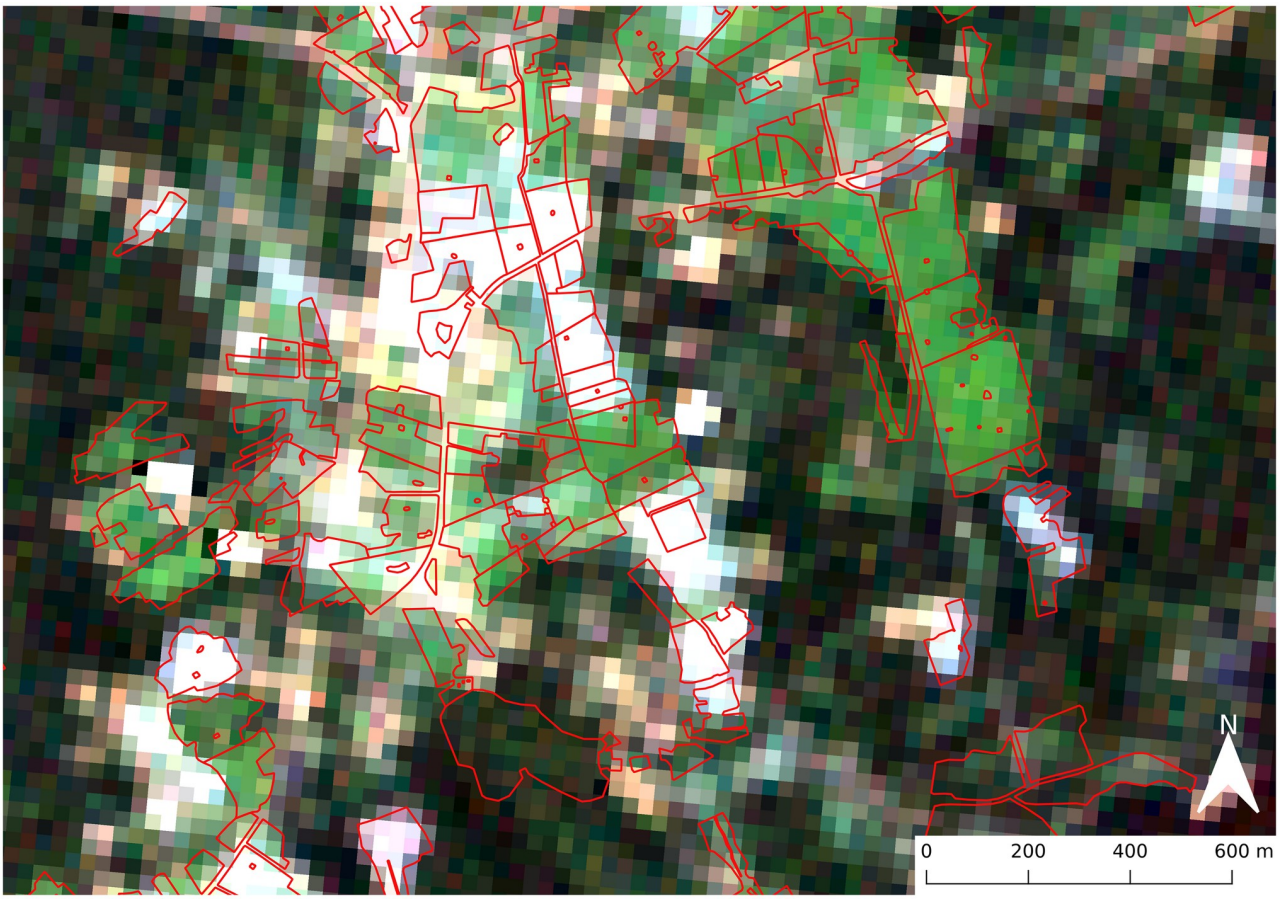

Fig 3. Field parcel example. Example area with field parcels boundaries (red) fromthe year 2012 (open data:http://www.nic.funet.fi/index/geodata/mavi/peltolohkot/2012/, accessed 28.09.21) andLandsat 7 true color image from 03.08.01 in the background (location: Western Finland,green arrow in Fig 2).

https://doi.org/10.1371/journal.pone.0251952.g003

and one panchromatic band. All bands are provided with a spatial resolution of 30 m except panchromatic and thermal infrared bands, which are provided with 15 m and 60 m resolution, respectively. The revisit time of the satellite to a specific point on earth is 16 days.

All available surface reflectance products [32] from January 2000 to December 2015 were requested from the United States Geological Survey (USGS) and downloaded using the EROS Processing Architecture software where EROS stands for Earth Resources Observation and Science. No filters were applied to the query other than the path and row indicators for the area of interest with least spatial overlap. The query resulted in 597 scenes. An overview of the number of scenes acquired per year can be found in Table 2. The surface reflectance product also includes a Quality Assessment (QA) band indicating the cloud cover based on the CFMask algorithm [33]. The QA band was used to generate a binary cloud mask. Note that, the surface reflectance product is not processed when the solar zenith angle is larger than 76 degrees. Thus data availability is limited, since the study area is above 60˚North.

In 2003, Landsat 7 experienced a scan line corrector malfunction, which influenced later acquisitions by introducing gaps with missing data in the scenes. However, field parcels in Finland are much smaller than this gap, and, therefore, no correction or filling of the gaps was performed. The gaps were interpreted as missing data for each field located within the gap.

Table 1. Percentage of field parcels for which crop loss was reported for each year.

year	#parcels	#parcels with loss	loss ratio (%)
2000	90,020	627	0.70
2001	85,592	2,227	2.60
2002	88,293	936	1.06
2003	86,387	1,311	1.52
2004	51,199	5,870	11.47
2005	96,503	414	0.43
2006	96,636	2,892	2.99
2007	68,599	125	0.18
2008	103,887	3,544	3.41
2009	103,315	91	0.09
2010	81,899	883	1.08
2011	85,097	1,056	1.24
2012	87,554	6,017	6.87
2013	94,583	488	0.52
2014	86,967	783	0.90
2015	112,341	6,576	5.85
Total	1,418,872	33,840	2.38

https://doi.org/10.1371/journal.pone.0251952.t001

2.3 Data preparation

All Landsat 7 scenes were processed to create a data set in the required format to train and test the classification models, by four steps: extracting image sequences, computing NDVI time series, aggregating NDVI across time and imputing missing data. Fig 5 schematically shows these steps, which are described in detail below.

2.3.1 Extracting image sequences. For each field parcel, the boundary information from the reference data was used to extract the corresponding image segments from the raster files. An image segment consists of all pixels within the field-parcel boundary. If a field parcel was in two Landsat 7 tiles, only one was kept to avoid overlap. This yielded a sequence of images (of seven bands—the six spectral bands and the pixel QA band) that were further processed to discard invalid pixels using the QA mask. These were mainly cloud pixels.

2.3.2 Computing NDVI time series. The multispectral images were used to compute Normalised Difference Vegetation Index (NDVI) band according to the formula:

$$\mathrm{NDVI} = \frac{\rho_{\mathrm{nir}} - \rho_{\mathrm{red}}}{\rho_{\mathrm{nir}} + \rho_{\mathrm{red}}}, \tag{1}$$

where ρ_{nir} and ρ_{red} are the pixel values of the near infrared (central wavelength 0.77–0.90 μm) and red (central wavelength 0.63–0.69 μm) bands, respectively. This process resulted in a sequence of NDVI images for each field parcel. From these (NDVI) image sequences, we get NDVI time series $\mathbf{x}''$ by taking the median (NDVI) pixel.

2.3.3 Aggregating NDVI across time. The temporal resolution of $\mathbf{x}''$ refers to the frequency at which Landsat 7 scenes were captured. This is mainly a function of revisit frequency (16 days) of the satellite and cloud cover. As a result, time series $\mathbf{x}''$ of different fields have different lengths and their time indices are not aligned. To address these two problems, we perform temporal averaging as follows: First, we form a new time scale from 1 to 365 (corresponding to each day of a year) within which each time series $\mathbf{x}''$ is located based on the time of capture. Then, the new time scale is divided into d bins. The NDVI values within each

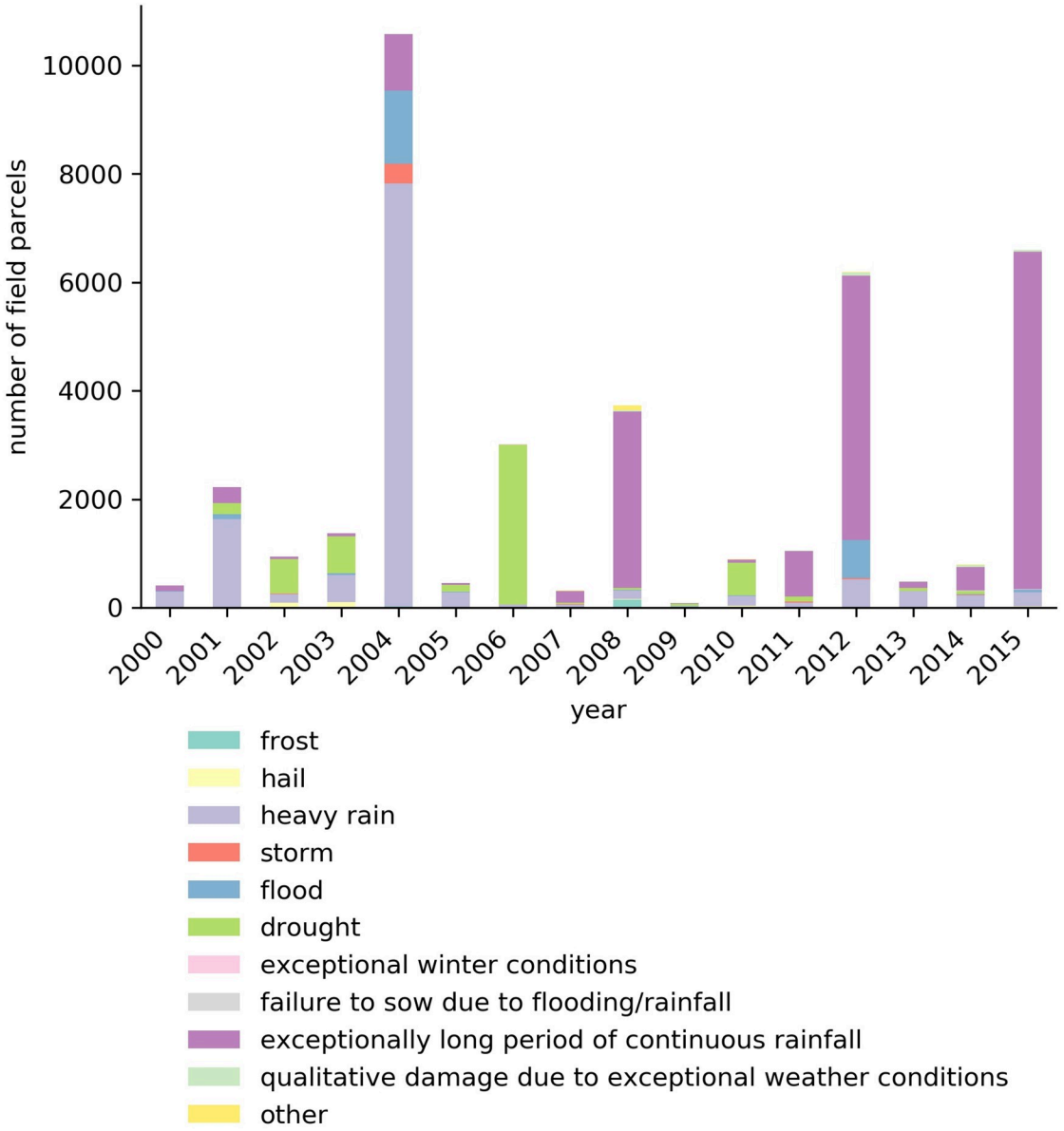

Fig 4. Reasons for crop loss of barley in Finland between 2000-2015. Percentage from total (33560) per type for all years: frost: 0.67%, hail: 0.79%, heavy rain: 25.70%, storm: 0.74%, flood: 5.45%, drought: 15.83%, exceptional winter conditions: 0.02%, failure to sow due to flooding or rainfall: 0.11%, exceptionally long period of continuous rainfall: 49.66%, qualitative damage caused over a large area due to exceptional weather conditions 0.53%, other: 0.50%.

https://doi.org/10.1371/journal.pone.0251952.g004

bin are the mean aggregated to yield a new time series $\mathbf{x}'$. We set $d = 12$, by which edges for 12 bins are given by $t_1 = [1, 30]$, $t_2 = [31, 36]$, $t_3 = [61, 90]$, . . ., $t_{12} = [331, 360]$. Some example time series $\mathbf{x}'$ are shown in Fig 6, where red and blue lines represent fields with and without crop loss, respectively. It can be seen that, unlike a typical time series, there are many holes in $\mathbf{x}'$. That is, even after temporal averaging the time series of each field parcel has many missing values. If we take the average of all the red and all the blue curves, then we see a general pattern of the aggregated NDVI time series for the two classes as shown in Fig 7. In each year, the top-right value shows the Pearson correlation (referred to as NDVI-corr) between the red and blue curves, indicating a high correlation between them in each year. These high correlations imply

Table 2. Number of Landsat 7 ETM+ surface reflectance products acquired per year (January—December) per tile (cf. Fig 2 for location of tiles).

year/tile	18718	18918	19015	19017	19116
2000	15	14	13	16	15
2001	10	13	10	11	10
2002	11	13	10	11	12
2003	9	7	5	6	4
2004	4	4	2	1	4
2005	5	5	4	4	5
2006	5	4	4	5	2
2007	3	4	1	1	6
2008	4	6	5	5	6
2009	6	8	5	6	5
2010	4	5	4	3	4
2011	5	8	6	9	8
2012	6	11	6	7	10
2013	11	10	7	8	11
2014	7	8	11	11	9
2015	14	13	10	14	12

https://doi.org/10.1371/journal.pone.0251952.t002

the hardness of classifying the parcels into those with loss or without loss. NDVI-corr is used later in Section 3.2 for exploring the factors to explain classification performance.

2.3.4 Imputing missing data. *2.3.4.1 Missing data problem*. Missing data is a common problem when dealing with satellite images due to cloud cover and other data acquisition problems. This is especially problematic for northern countries like Finland due to the low sun angle. In ideal circumstances such as no cloud cover and no acquisition problems, the time series length is approximately 22 time steps (assuming an average revisit period is 16 days for Landsat 7). However, in our case, the average length of the time series is 4 due to missing data, i.e., around 82% of the data is missing. Fig 8 shows the missing data profile for different years. In some years e.g. 2003 and 2004, the problem is more severe where more than 90% of the data are missing. We observe that for all the years, the data in the beginning and end of the year are likely to be missing. This phenomenon can be explained by the low illumination angle during winter for which no surface reflectance product is processed. For barley, these missing data points during winter should have little effect since its heading time is around beginning of July, while maturity is reached around the middle of August in this part of Finland [34]. We also see that the pattern of missing data is different for the two classes in all years, suggesting that information on the location of missing values can help improving the classification.

2.3.4.2 Imputation methods for missing data. We address the missing data problem in $\mathbf{x}'$ through mean imputation (`Mean`). The procedure is described using the following matrix notation for clarity. The time series $\mathbf{x}'$ of all the fields form a matrix $\mathbf{X}'$ where columns are the new time indices described in Section 2.3.3 and the missing entries correspond to the holes in the times series. These missing values are filled by the corresponding column mean of $\mathbf{X}'$ yielding the matrix $\mathbf{X}$. Each row $\mathbf{x}_i$ in the matrix $\mathbf{X}$ is the imputed time series of the field *i*.

Apart from mean imputation we also experiment with two other imputation methods: 1) missing data indicator (`MI`), and 2) multiple imputation by chained equation (`MICE`). `MI` generates a binary matrix $\mathbf{M}$ of the same size as the data matrix $\mathbf{X}$, indicating the absence of a value. `MICE` is an iterative method which regresses each variable (column of $\mathbf{X}'$) over the other

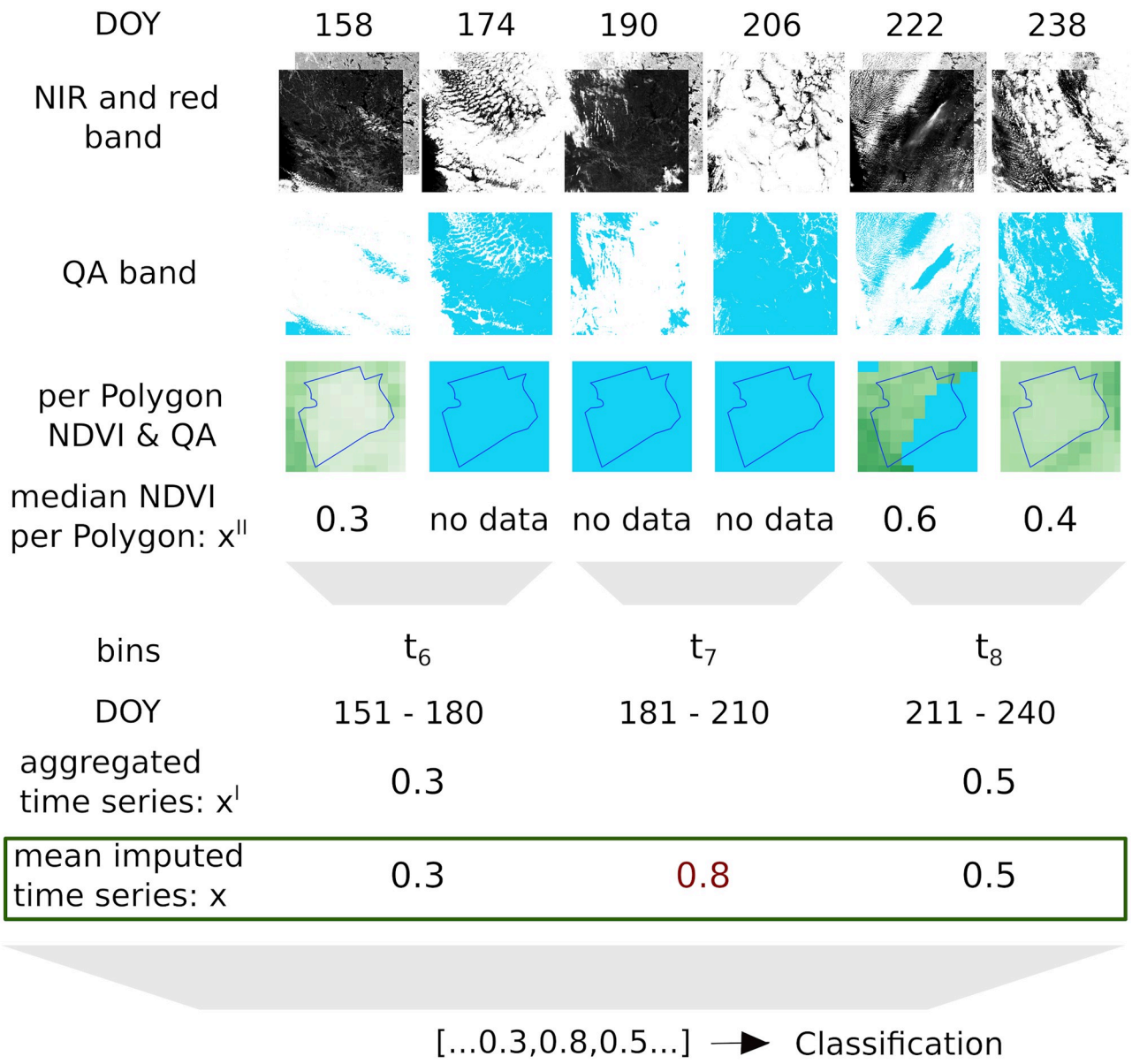

Fig 5. Data preparation workflow. Workflow (top to bottom) of computing time series **x** (= (0.3, 0.8, 0.5) in the green box), starting from raw Landsat 7 scenes (top) for part of a time series (DOY 158-238 2000). The 0.8 (marked in red) is the imputed mean value (of all other fields at the same time point) for t_7. In the end, the time series is forwarded to the classification as independent features. DOY: day of year, NIR: near infrared and QA: Quality Assessment/cloud mask.

https://doi.org/10.1371/journal.pone.0251952.g005

in a round-robin fashion to compute the missing values [35]. These methods are compared in Section 3.1 to identify the best imputation strategy for classification. The imputation methods in Scikit-learn library [36] were used for the experiments.

Note that due to the severity of missing data, time series interpolation methods to fill the missing values were not considered. This is because the time series were short (average length is 4) with many instances consisting of only one or two observations. In these cases interpolation is not meaningful. Instead different imputation methods were considered to fill the missing values.

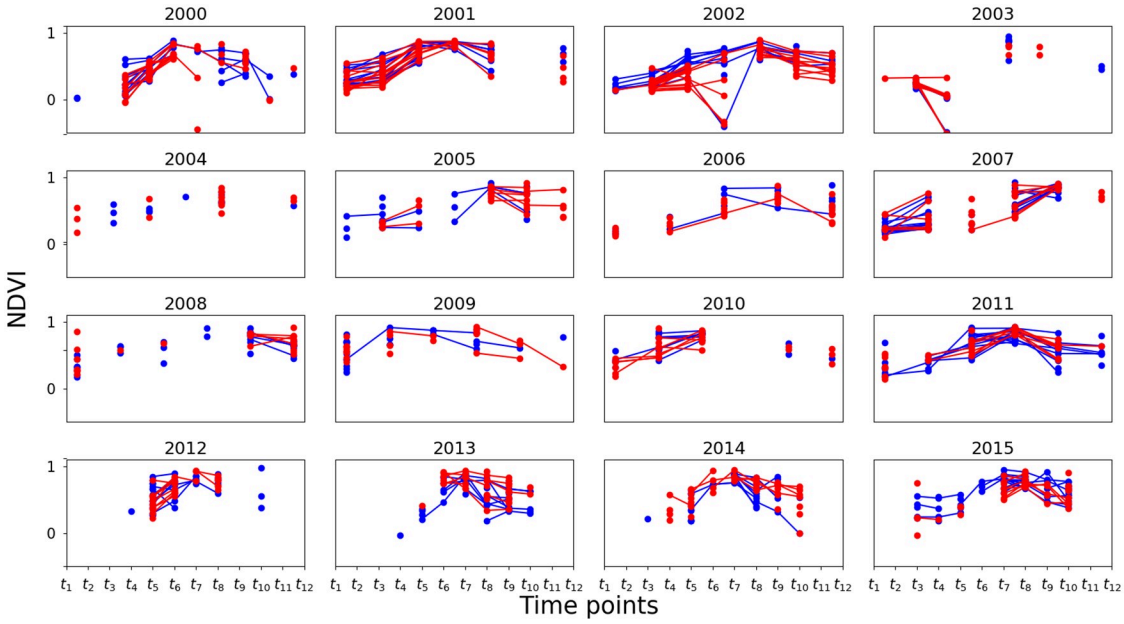

Fig 6. NDVI time series examples. Time series plots for some example field parcels with and without crop loss in red and blue, respectively. Note that the lack of lines between the points is due to the missing values.

https://doi.org/10.1371/journal.pone.0251952.g006

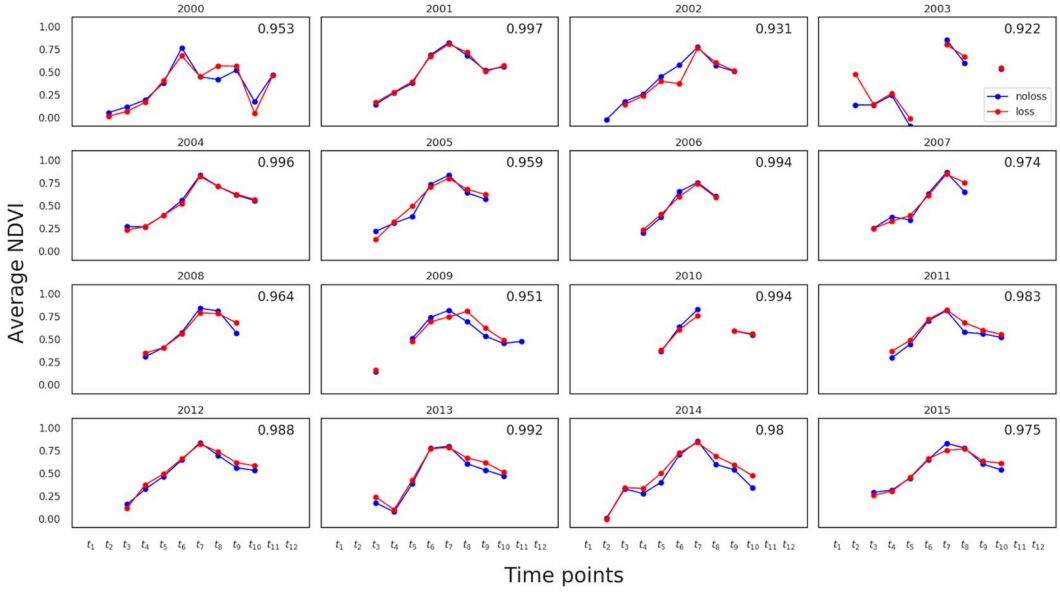

Fig 7. Average NDVI time series. Average NDVI time series of each year for each class (red = loss, blue = no-loss). The top-right (NDVI-corr) value in each year shows the Pearson correlation between the two curves.

https://doi.org/10.1371/journal.pone.0251952.g007

2.4 Classification models

Given data set $\{\mathcal{D} = (\mathbf{x}_i, y_i)\}_{i=1}^{n}$ with n observations, the task is to learn a model f: $\mathbf{x} \mapsto y$ such that $p(y_i) = f(\mathbf{x}_i;\theta)$ where θ is a set of hyperparameters. We compared several classification models namely Logistic Regression (`LR`), Decision Trees (`DT`), Random Forest (`RF`) and Multilayer Perceptrons (`MLP`) [36]. Due to a large amount of missing data, which makes time series

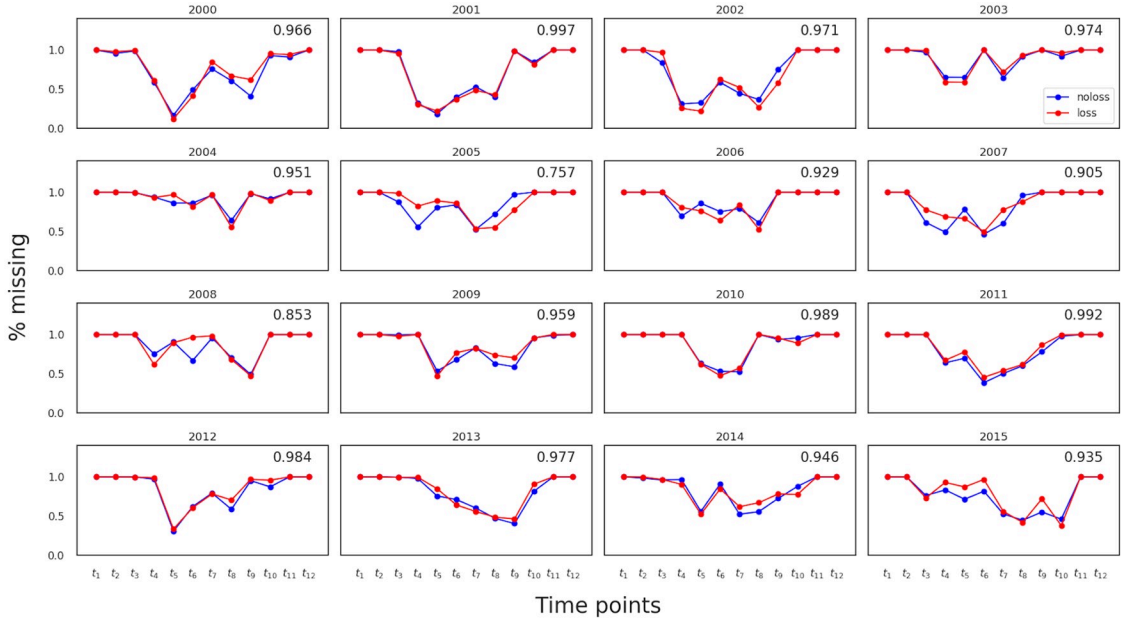

Fig 8. Missing data profile. Percentage of field parcels with missing values on the y-axis vs time point on the x-axis. The red and blue curves indicate crop loss and no crop loss, respectively. The top-right value in each year shows the Pearson correlation between the two curves, referred to as MD-corr (used later in Section 3.2).

https://doi.org/10.1371/journal.pone.0251952.g008

very short, we model the time points as independent features, and did not consider time series models (such as autoregressive models or recurrent neural networks) in this work. All models are implemented using Scikit-learn (version 0.22.1) Python library [36] and the details of their optimisation and model comparison is given in Section 3.1.

To compare the models, we focused on the data from year 2015 because it has the least amount of missing data (see Fig 8). Also class imbalanceness in 2015 is relatively better than other years (see Table 1). We then created a balanced data set (with 13,152 fields), with all 6,576 crop-loss fields and the equal number of no-crop-loss fields (which were sampled out of all no-crop-loss parcels by means of undersampling). This balanced data set was used for cross-validation only for the model comparison.

Before comparing the models, we first optimised the hyperparameters of each model. Table 3 shows hyperparameters that were optimised, along with their respective ranges considered and the optimal values. The results are detailed in Section 3.1

2.5 Performance metrics

The performance measure used to evaluate the classification models was "area under the receiver operating characteristic (ROC) curve" (AUC) [38]. AUC takes a value in the interval

Table 3. Model hyperparameters, their ranges and optimal values obtained.

Model	Parameters and Range	Optimal value
LR	regularisation penalty = {1, 10}	1
DT	maximum tree depth = {5, 10, 50}	5
RF	maximum tree depth = {5, 10, 50}	10
	#trees = {10, 50 }	50
MLP	#hidden units = {10, 5 }	10

https://doi.org/10.1371/journal.pone.0251952.t003

[0, 1], where a random classifier has a score of around 0.5 and a perfect classifier has score 1. AUC is insensitive to class imbalance which is important for this study as class imbalance is high. Further, it has a standard scale independent of the number of data points and the distribution of classes, so models trained on data from different years are directly comparable even though the number of loss and no-loss fields are different in each year. We used 10×10-fold cross-validation (CV) to compute the AUC of each model in all experiments (except in Section 3.3): In K-fold cross-validation first the data into K non-overlapping folds. Then the model is trained on $K - 1$ folds and tested on the remaining fold. This is repeated K times so that model is tested on each of the K folds. The model performance is given by average of the K AUC values. We used $K = 10$ and repeat 10-fold cross-validation 10 times with different random permutation of the data.

2.6 Within-year classification

Within-year classification situation is to determine if there was a crop loss in a field (for which the crop loss information was unavailable in a year), by using fields for which crop loss data are available in the same year. We used all data of each year for cross-validation, meaning training and test parcels being from the same year. The AUC value for each year is computed using the 10x10 cross-validation procedure described in Section 2.4 to compute the AUC values for each year.

2.7 Between-year classification

Collecting reference data is expensive so it would be useful to identify crop-loss fields in a year based on reference data from a different year(s). This *between-year classification* situation would be closer to future prediction of crop loss in a field, more than within-year classification. We considered two cases: single-year training and multiple-year training. For single year training case, all data from one year was used for training while all data from another year was used for testing. In the multiple year training case, test data are taken from one year and training data are taken from the remaining 15 years. For example, if test data is taken from 2015 then training data are taken from 2000 to 2014. Note that cross-validation was not used for between-year classification.

3 Results

3.1 Model comparison

We first compared machine learning models and imputation methods, to find the most appropriate model and imputation strategy to be used throughout this work. As part of identifying the optimal imputation strategy, we also decide whether or not to include indicators specifying the locations of missing values as part of the input to the model.

Table 4 shows AUCs for the different combinations of the model and imputation strategy. The method with the highest AUC was the combination of `RF` and `Mean+MI` (mean

Table 4. Mean AUC of 10x10-fold CV for different models and imputation methods.

	Mean	Mean+MI	MICE	MICE+MI
LR	0.6903 ± 0.009	0.7377 ± 0.008	0.6473 ± 0.010	0.7128 ± 0.008
DT	0.7080 ± 0.008	0.7187 ± 0.007	0.6364 ± 0.010	0.7223 ± 0.008
MLP	0.7322 ± 0.009	0.7546 ± 0.008	0.6458 ± 0.010	0.7469 ± 0.008
RF	0.7514 ± 0.008	**0.7602 ± 0.008**	0.6515 ± 0.010	0.7505 ± 0.008

https://doi.org/10.1371/journal.pone.0251952.t004

Table 5. Ratio of training time of four models relative to RF.

	Mean	Mean+MI	MICE	MICE+MI
LR	0.03	0.05	10.12	10.03
DT	0.04	0.05	10.36	10.36
MLP	12.21	10	15.91	20.51
RF	0.97	**1**	11.42	11.88

https://doi.org/10.1371/journal.pone.0251952.t005

imputation and missing value indicators), followed by the pair of MLP and Mean+MI. Table 5 shows computation time of different methods, indicating the significant computational advantage of Mean and Mean+MI over MICE. Focusing on Mean+MI, we further studied model comparison over all 15 years (see Appendix Table 5 in detail). From this result, although RF and MLP were overall the two most accurate methods, taking computation time into account, we concluded that the combination of RF and Mean+MI is the recommended model for crop-loss classification, and used this combination for the remainder of the experiments in this study.

3.2 Within-year classification

Table 6 shows the within-year classification performance for 16 years. The average AUC across all years is 0.6884±0.027 with the best performance in 2008 with AUC = 0.795±0.008 and the worst in 2004 with AUC = 0.602±0.010. We investigated possible factors to explain the differences in those AUCs across years:

1. **NDVI correlations:** We first checked the correlation in NDVI between crop-loss and no-crop-loss fields, i.e. the correlation (NDVI-corr) between blue and red curves in Fig 7. Fig 9 shows a scatter plot of AUC against NDVI-corr for all years. We see that AUC decreases as NDVI-corr increases. For example, 2004 had the highest NDVI-corr = 0.996 and the lowest AUC = 0.602, whereas 2008 had the lowest NDVI-corr = 0.964 and the highest AUC = 0.795.

Table 6. Within-year classification performance (AUC) for all the years.

Year	AUC
2000	0.757 ± 0.028
2001	0.648 ± 0.018
2002	0.765 ± 0.022
2003	0.706 ± 0.021
2004	0.602 ± 0.010
2005	0.750 ± 0.031
2006	0.657 ± 0.015
2007	0.627 ± 0.070
2008	**0.795 ± 0.008**
2009	0.647 ± 0.070
2010	0.624 ± 0.027
2011	0.673 ± 0.023
2012	0.636 ± 0.010
2013	0.679 ± 0.033
2014	0.690 ± 0.292
2015	0.755 ± 0.008
Mean	0.684 ± 0.027

https://doi.org/10.1371/journal.pone.0251952.t006

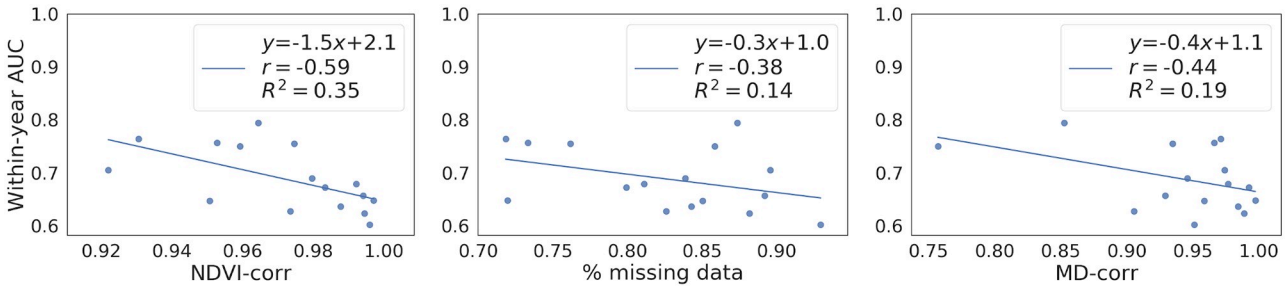

Fig 9. Analysis of AUC values. Effect of NDVI-corr (left), % missing data (middle) and MD-corr (right) on AUC of within-year classification. The Pearson correlation between the quantities are given by r in the top right corner of the each plot. The regression line and R^2 are included for illustrative purpose only to highlight the inverse relationship between the quantities.

https://doi.org/10.1371/journal.pone.0251952.g009

2. **Amount of missing data:** We then examined the impact of missing data on AUC. Fig 9 plots AUC against the percentage of missing data per year, where AUC decreased with increasing amount of missing data. The linear regression line, $y = -0.3x + 1.0$, indicates that the classification performance can improve when the amount of missing data reduces.

3. **Missing data profile correlations:** We further checked the similarity in missing data profiles of two classes by using MD-corr. Fig 9 plots AUC against MD-corr, showing that AUC decreases with MD-corr is increasing, meaning that not only the amount of missing data but also the pattern of missing data affects classification performance.

We thus can see NDVI correlation, missing data ratio and missing data profile correlation, are important factors in the data that affect classification performance. Also we hypothesise that similar missing data patterns may indirectly indicate similar weather conditions or geographical closeness of different fields, which might be useful for classification. We note that using missing data indicators as input to the classification model will be feasible in practice, as those will be available for the application at the same time as the satellite images themselves. However, missing data can be based on many reasons, such as cloud cover, data not processed to surface reflectance and scan line error so we cannot draw a causal relationship between the missingness pattern and crop-loss even when the classification accuracy is high.

3.2.1 Impact of field parcel area. We further examined the potential impact of field area on within-year classification, since larger fields are more likely to be crop-loss fields and this bias may affect classification performance. For this experiment, we focused on data from 2004, 2008, 2012 and 2015 (each had >3% crop-loss fields; see Table 1), to ensure that the class imbalance problem is not exacerbated when the data is divided based on the area. The field parcels are divided into three groups, depending on their area: small (< 1ha), medium (≥1ha and <3ha), and large (≥3ha). Table 7 shows the number of fields in the three groups for these four years. Table 8 shows the performance results, indicating that in each year, AUCs were approximately consistent with those obtained by using all data in Table 6 (2004: 0.602, 2008:

Table 7. Ratio (%) of crop loss parcels for three groups with different areas and four years.

	#parcels	#parcels with loss	small ratio (%)	#parcels	#parcels	medium ratio (%)	#parcels	#parcels with loss	large ratio (%)
2004	15,050	1,676	11.13	22,267	2,511	11.28	13,882	1,683	12.12
2008	30,948	920	2.97	43,935	1,444	3.29	29,004	1,180	4.07
2012	25,282	1,558	6.19	36,532	2,537	6.94	25,841	1,922	7.44
2015	31,112	1,548	4.98	44,998	2,570	5.71	36,231	2,458	6.78

https://doi.org/10.1371/journal.pone.0251952.t007

Table 8. Within-year AUC of three groups with different field parcel sizes.

Year	small	medium	large
2004	0.6071 ± 0.021	0.5878 ± 0.009	0.5938 ± 0.019
2008	0.8118 ± 0.018	0.7947 ± 0.010	0.7580 ± 0.014
2012	0.6314 ± 0.026	0.6387 ± 0.017	0.6237 ± 0.020
2015	0.7605 ± 0.023	0.7600 ± 0.010	0.7386 ± 0.015

https://doi.org/10.1371/journal.pone.0251952.t008

0.795, 2012: 0.636 and 2015: 0.755) and AUCs in different groups were close to each other. Hence, the field size would not play a significant role in the results.

3.3 Between-year classification

3.3.1 Single-year training. Fig 10 visualises totally 240 AUCs of all combinations of sixteen years, by using a heat map. Many AUC values were close to 0.5, and the average AUC = 0.534 ± 0.051. The maximum AUC was 0.665 (2003 for training and 2005 for testing) which is less than the average within-year AUC = 0.688. These results indicate that training data with only one year might not be informative enough for identifying parcels with crop loss in between-year classification.

3.3.2 Multiple-year training. Table 9 shows sixteen AUC values (one for each test year) obtained by this procedure, along with the corresponding average and best AUCs of single-year training. We can see several years in which multiple-year AUC can be better than the average single-year AUC, but for all years, multiple-year AUC is always worse than the best single-year AUC. This result implies that combining data from multiple years will not improve between-year classification.

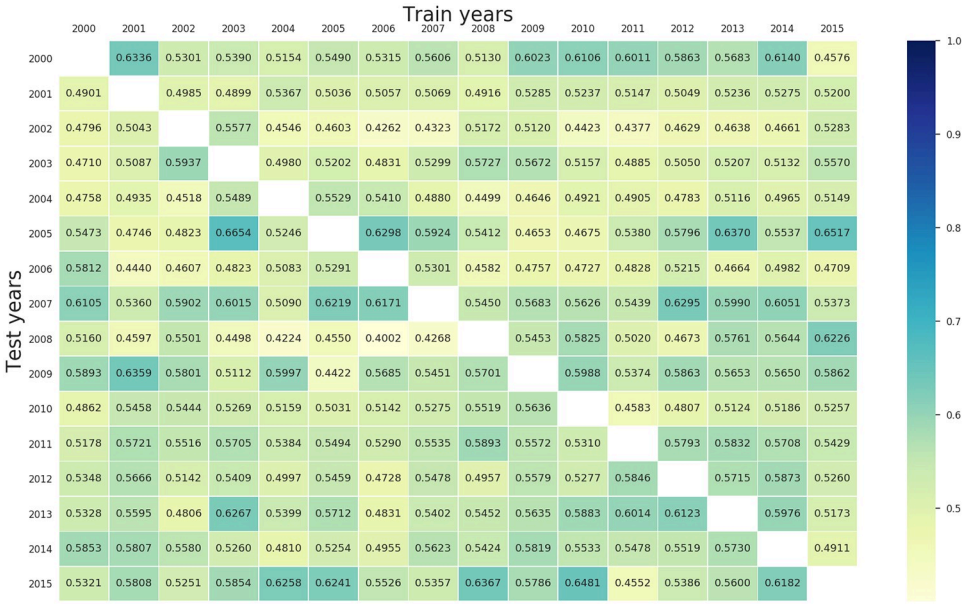

Fig 10. AUC values of single-year training experiment. The column and row heading indicates the year on which the model is trained and tested, respectively.

https://doi.org/10.1371/journal.pone.0251952.g010

Table 9. Multiple year training vs single year training (AUC).

Year	Multiple year	Single year (average)	Single year (best)
2000	0.6329	0.5608 ± 0.047	0.6335
2001	0.5226	0.5111 ± 0.015	0.5367
2002	0.4582	0.4764 ± 0.039	0.5576
2003	0.5319	0.5230 ± 0.035	0.5936
2004	0.5227	0.4967 ± 0.032	0.5529
2005	0.6287	0.5567 ± 0.068	0.6654
2006	0.4710	0.4921 ± 0.036	0.5811
2007	0.6362	0.5785 ± 0.037	0.6295
2008	0.6018	0.5027 ± 0.068	0.6226
2009	0.5703	0.5654 ± 0.044	0.6358
2010	0.5818	0.5184 ± 0.028	0.5636
2011	0.5423	0.5557 ± 0.021	0.5892
2012	0.4999	0.5382 ± 0.033	0.5872
2013	0.5548	0.5573 ± 0.043	0.6267
2014	0.5826	0.5437 ± 0.033	0.5853
2015	0.6093	0.5731 ± 0.052	0.6480

https://doi.org/10.1371/journal.pone.0251952.t009

4 Discussion

We have trained machine learning models to classify field parcels with and without crop loss, using NDVI values derived from Landsat 7 data. Several models were compared and tested in two different scenarios, namely within-year and between-year classification. The results showed that within-year classification is highly possible, while between-year classification is still hard. The resulting models have many applications, for example, they can be used by insurance companies or government agencies for verifying crop-loss claims. However, their performance will be contingent upon the availability of good reference data that captures all possible variations in environmental and biophysical conditions.

Our study showed that a major challenge to improve the classification performance is the amount of missing data. Fig 9 shows the possibility of achieving high AUC if the missing data ratio was low. In our case more than 80% of data are missing and despite that the average within-year AUC = 0.688 with the possibility to increasing up to 90% when the problem is not severe. The issue might be improved by using newer spaceborne multispectral data, such as those from Sentinel 2 which has higher temporal and spatial resolution that could mitigate the effect of missing data. Furthermore, Sentinel 2 data can be combined with RADAR data from Sentinel 1 to get a denser time series and avoid occlusion from clouds to provide more detailed information about the growing pattern of agricultural fields. Obviously, such data are available only from the most recent years, and therefore cannot be combined with our crop loss data, which had covered many years but until 2015.

Between-year classification allows identification of crop-loss fields without any reference data in the same year so improving its performance would be a good future target. Our result in Section 3.3 implies that NDVI data alone might not be sufficient for improving the performance of between-year classification. Incorporating temperature and precipitation data along with the crop-loss reasons can give a more complete picture of the factors affecting the crop loss. Based on the promising results of within-year classification, augmenting high resolution satellite data with weather variables would be useful in achieving high performance for between-year classification.

Another direction in which our work could be extended is the use of more flexible machine learning models. For example, convolutional neural networks could use the full image as input and recurrent neural networks could explicitly model the time dependency. These models have the potential to increase the classification performance. However, these models require a large amount of data to train properly, and cannot be directly applied to our data, which has a huge amount of missing data and consists of relatively short time series. The machine learning models in our study are rather simpler as they are more robust against the limitations in our data.

5 Conclusion

We have proved the feasibility of training a machine learning model to identify crop loss at field parcel scale using NDVI data derived from Landsat 7 satellite images. Experiments across sixteen years showed that field parcels from a given year can be classified into those with and without crop loss when the model can be trained on data from the same year. However, the ability to classify parcels from other years is limited. Missing data, which occupied more than 80% of our satellite images, deteriorated the classification performance. Preliminary analysis indicated that within-year classification performance can be improved if the missing data ratio was reduced. As long as we can assume that the NDVI times series of barley crop is similar with minor variation due to environmental and biophysical conditions then we believe that findings of this study can be generalised to barley fields in other countries.

6 Appendix

6.1 Model comparison for all years

In Section 3.1, we performed model comparison on 2015 data to determine the best model. Table 10 extends these results to the other 15 years. Here all models were implemented with `Mean+MI` imputation strategy. We see that for all years, `RF` and `MLP` have have similar AUC values and outperform `DT` and `LR`. However, `MLP` was less robust that `RF`, i.e., it did not converge even after 500 iterations for several years (2005, 2007, 2009, 2011, 2013, 2014) and took

Table 10. AUC of different models with `Mean+MI` imputation strategy.

Year	RF	MLP	DT	LR
2000	**0.7643 ± 0.029**	0.7471 ± 0.037	0.6662 ± 0.044	0.7139 ± 0.046
2001	**0.6509 ± 0.021**	0.6409 ± 0.018	0.5735 ± 0.018	0.6223 ± 0.023
2002	0.7555 ± 0.036	**0.7582 ± 0.025**	0.6771 ± 0.053	0.7051 ± 0.031
2003	**0.6954 ± 0.032**	0.6779 ± 0.029	0.6602 ± 0.028	0.6625 ± 0.028
2004	0.5920 ± 0.015	**0.5943 ± 0.015**	0.5721 ± 0.012	0.5849 ± 0.007
2005	**0.7699 ± 0.034**	0.7552 ± 0.030	0.6935 ± 0.041	0.7452 ± 0.038
2006	0.6624 ± 0.021	**0.6632 ± 0.024**	0.6176 ± 0.026	0.6392 ± 0.025
2007	0.6844 ± 0.097	**0.7048 ± 0.101**	0.6029 ± 0.105	0.6824 ± 0.088
2008	0.7840 ± 0.012	**0.7871 ± 0.012**	0.7474 ± 0.012	0.7667 ± 0.016
2009	0.7146 ± 0.133	**0.7548 ± 0.087**	0.6242 ± 0.124	0.7046 ± 0.084
2010	0.6418 ± 0.031	**0.6549 ± 0.036**	0.6085 ± 0.024	0.6478 ± 0.041
2011	**0.6839 ± 0.054**	0.6708 ± 0.058	0.6333 ± 0.049	0.6624 ± 0.050
2012	**0.6360 ± 0.016**	0.6344 ± 0.014	0.5985 ± 0.015	0.6169 ± 0.020
2013	**0.6771 ± 0.050**	0.6729 ± 0.049	0.6354 ± 0.052	0.6888 ± 0.060
2014	**0.7213 ± 0.030**	0.7103 ± 0.035	0.6315 ± 0.046	0.6959 ± 0.032

https://doi.org/10.1371/journal.pone.0251952.t010

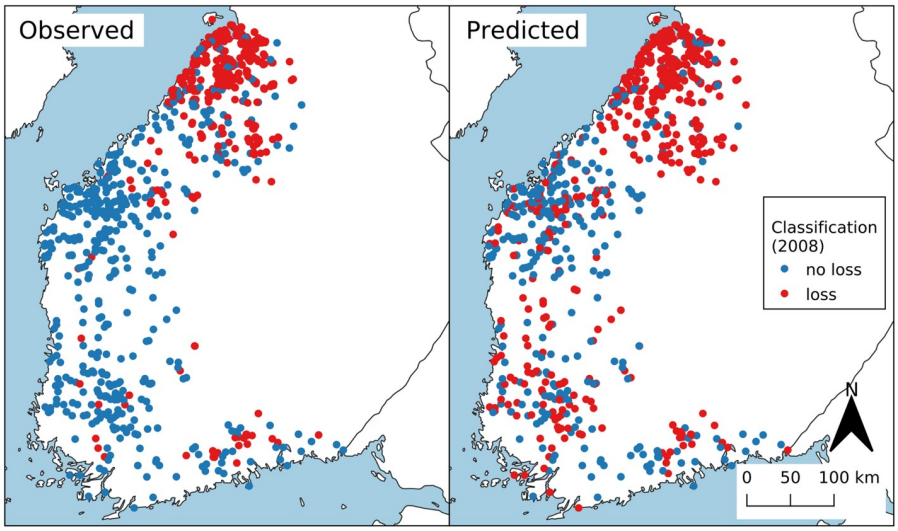

Fig 11. Classification result. Observed (left) vs predicted (right) crop loss of 1000 randomly chosen field parcels in 2008 simplified as points. Red point indicates croploss of the fieldparcel, blue point indicates no loss in 2008.

https://doi.org/10.1371/journal.pone.0251952.g011

longer to train (Table 5). Thus, considering performance, stability and training time, we selected `RF` for further experiments.

6.2 Visualising within-year classification results

Fig 11 shows the observed and predicted crop loss of 1000 field parcels for 2008. We choose 2008 because it has 1) 'sufficient' number of crop-loss parcels to divide into train and test sets, 2) relatively low missing data and 3) highest AUC. The following procedure was used to generate the plot. First data was randomly split into two sets: train and test. The test set consisted of 500 random crop-loss and 500 random no-crop-loss field parcels. All the remaining data formed the train set that was used to train the model (combination of `RF` and `Mean+MI`). Then the ROC curve of the trained model was analysed and the 'optimal' classification threshold determined to be the one that maximises the sensitivity and specificity of the model (also called Youden's J-index [39]). Finally, the trained model and the classification threshold was used to classify the field parcels in the test set. It should be noted that Youden's J-index is just one way to determine the optimal operating point on the ROC curve. An optimal point of a classifier is a trade-off between the cost of detecting false positives against the cost of failing to detect positive which is always application dependent.

Author Contributions

Conceptualization: Santosh Hiremath, Samantha Wittke, Taru Palosuo, Jere Kaivosoja, Fulu Tao, Pirjo Peltonen-Sainio, Pekka Marttinen, Hiroshi Mamitsuka.

Data curation: Santosh Hiremath, Samantha Wittke, Jere Kaivosoja, Maximilian Proll.

Funding acquisition: Pirjo Peltonen-Sainio, Pekka Marttinen, Hiroshi Mamitsuka.

Investigation: Samantha Wittke, Jere Kaivosoja.

Methodology: Santosh Hiremath.

Project administration: Pekka Marttinen, Hiroshi Mamitsuka.

Resources: Fulu Tao, Pekka Marttinen, Hiroshi Mamitsuka.

Software: Santosh Hiremath, Samantha Wittke.

Supervision: Eetu Puttonen, Pekka Marttinen, Hiroshi Mamitsuka.

Validation: Santosh Hiremath, Samantha Wittke.

Visualization: Santosh Hiremath, Samantha Wittke.

Writing – original draft: Santosh Hiremath, Samantha Wittke.

Writing – review & editing: Santosh Hiremath, Samantha Wittke, Taru Palosuo, Jere Kaivosoja, Fulu Tao, Eetu Puttonen, Pirjo Peltonen-Sainio, Pekka Marttinen, Hiroshi Mamitsuka.

References

1. Weiss M, Jacob F, Duveiller G. Remote sensing for agricultural applications: A meta-review. Remote Sensing of Environment. 2020; 236:111402. https://doi.org/10.1016/j.rse.2019.111402
2. Boryan C, Yang Z, Mueller R, Craig M. Monitoring US agriculture: the US Department of Agriculture, National Agricultural Statistics Service, Cropland Data Layer Program. Geocarto International. 2011; 26:341–358. https://doi.org/10.1080/10106049.2011.562309
3. Becker-Reshef I, Justice C, Sullivan M, Vermote E, Tucker C, Anyamba A, et al. Monitoring global croplands with coarse resolution earth observations: global agriculture monitoring (GLAM) project. Remote Sensing. 2010; 2:1589–1609. https://doi.org/10.3390/rs2061589
4. Gitelson AA, Viña A, Arkebauer TJ, Rundquist DC, Keydan G, Leavitt B. Remote estimation of leaf area index and green leaf biomass in maize canopies. Geophysical Research Letters. 2003; 30(5). https://doi.org/10.1029/2002GL016450
5. Wiseman G, McNairn H, Homayouni S, Shang J. RADARSAT-2 polarimetric SAR Response to crop biomass for agricultural production monitoring. IEEE Journal of Selected Topics in Applied Earth Observations and Remote Sensing. 2014; 7:4461–4471. https://doi.org/10.1109/JSTARS.2014.2322311
6. Mulla DJ. Twenty five years of remote sensing in precision agriculture: key advances and remaining knowledge gaps. Biosystems Engineering. 2013; 114:358–371. https://doi.org/10.1016/j.biosystemseng.2012.08.009
7. Toureiro C, Serralheiro R, Shahidian S, Sousa A. Irrigation management with remote sensing: evaluating irrigation requirement for maize under mediterranean climate condition. Agricultural Water Management. 2017; 184:211–220. https://doi.org/10.1016/j.agwat.2016.02.010
8. Bolton DK, Friedl MA. Forecasting crop yield using remotely sensed vegetation indices and crop phenology metrics. Agricultural And Forest Meteorology. 2013; 173:74–84. https://doi.org/10.1016/j.agrformet.2013.01.007
9. Azzari G, Jain M, Lobell DB. Towards fine resolution global maps of crop yields: Testing multiple methods and satellites in three countries. Remote Sensing of Environment. 2017; 202:129–141. https://doi.org/10.1016/j.rse.2017.04.014
10. Idso SB, Jackson RD, Reginato RJ. Remote sensing of crop yields. Science. 1977; 196:19–25. https://doi.org/10.1126/science.196.4285.19 PMID: 17733505
11. Awad M. Toward precision in crop yield estimation using remote sensing and optimization techniques. Agriculture. 2019; 9(3):54. https://doi.org/10.3390/agriculture9030054
12. Jin Z, Azzari G, Lobell DB. Improving the accuracy of satellite-based high-resolution yield estimation: A test of multiple scalable approaches. Agricultural and Forest Meteorology. 2017; 247:207–220. https://doi.org/10.1016/j.agrformet.2017.08.001
13. Basso B, Liu L. Seasonal crop yield forecast: methods, applications, and accuracies. In: Advances in Agronomy. vol. 154. Elsevier; 2019. p. 201–255.
14. Tapia-Silva FO, Itzerott S, Foerster S, Kuhlmann B, Kreibich H. Estimation of flood losses to agricultural crops using remote sensing. Physics and Chemistry of the Earth, Parts A/B/C. 2011; 36:253–265. https://doi.org/10.1016/j.pce.2011.03.005
15. Di L, Yu EG, Kang L, Shrestha R, Bai YQ. RF-CLASS: A remote-sensing-based flood crop loss assessment cyber-service system for supporting crop statistics and insurance decision-making. Journal of Integrative Agriculture. 2017; 16:408–423. https://doi.org/10.1016/S2095-3119(16)61499-5

16. Yang MD, Huang KS, Kuo YH, Tsai HP, Lin LM. Spatial and spectral hybrid image classification for rice lodging assessment through UAV imagery. Remote Sensing. 2017; 9. https://doi.org/10.3390/rs9060583

17. Ortiz-Monasterio JI, Lobell DB. Remote sensing assessment of regional yield losses due to sub-optimal planting dates and fallow period weed management. Field Crops Research. 2007; 101:80–87. https://doi.org/10.1016/j.fcr.2006.09.012

18. Sawant S, Mohite J, Sakkan M, Pappula S. Near real time crop loss estimation using remote sensing observations. In: 2019 8th International Conference on Agro-Geoinformatics (Agro-Geoinformatics); 2019. p. 1–5.

19. Silleos N, Perakis K, Petsanis G. Assessment of crop damage using space remote sensing and GIS. International Journal Of Remote Sensing. 2002; 23:417–427. https://doi.org/10.1080/01431160110040026

20. Ajadi OA, Liao H, Jaacks J, Delos Santos A, Kumpatla SP, Patel R, et al. Landscape-Scale Crop Lodging Assessment across Iowa and Illinois Using Synthetic Aperture Radar (SAR) Images. Remote Sensing. 2020; 12(23):3885. https://doi.org/10.3390/rs12233885

21. Hosseini M, Kerner HR, Sahajpal R, Puricelli E, Lu YH, Lawal AF, et al. Evaluating the Impact of the 2020 Iowa Derecho on Corn and Soybean Fields Using Synthetic Aperture Radar. Remote Sensing. 2020; 12(23):3878. https://doi.org/10.3390/rs12233878

22. Meuwissen MPM, Assefa TT, van Asseldonk MAPM. Supporting Insurance in European Agriculture: Experience of Mutuals in the Netherlands. EuroChoices. 2013; 12(3):10–16. https://doi.org/10.1111/1746-692X.12034

23. Liesivaara P, Myyrä S. Feasibility of an Area-Yield Insurance Scheme in the EU: Evidence from Finland. EuroChoices. 2015; 14(3):28–33. https://doi.org/10.1111/1746-692X.12096

24. Commission E. Overview of CAP reform 2014-2020; 2013. Available from: https://ec.europa.eu/info/sites/info/files/food-farming-fisheries/farming/documents/agri-policy-perspectives-brief-05_en.pdf.

25. European Commission. The future of rural development policy; 2011. Available from: https://ec.europa.eu/info/sites/info/files/food-farming-fisheries/farming/documents/agri-policy-perspectives-brief-04_en.pdf.

26. Peltonen-Sainio P, Rajala A. Use of quality seed as a means to sustainably intensify northern European barley production. The Journal of Agricultural Science. 2014; 152:93–103. https://doi.org/10.1017/S0021859612000962

27. Peltonen-Sainio P, Jauhiainen L, Sorvali J, Laurila H, Rajala A. Field characteristics driving farm-scale decision-making on land allocation to primary crops in high latitude conditions. Land Use Policy. 2018; 71:49–59. https://doi.org/10.1016/j.landusepol.2017.11.040

28. Peltonen-Sainio P, Jauhiainen L. Risk of low productivity is dependent on farm characteristics: how to turn poor performance into an advantage. Sustainability. 2019; 11:5504. https://doi.org/10.3390/su11195504

29. Peltonen-Sainio P, Venäläinen A, Mäkelä H, Pirinen P, Laapas M, Jauhiainen L, et al. Harmfulness of weather events and the adaptive capacity of farmers at high latitudes of Europe. Climate Research. 2016; 67:221–240. https://doi.org/10.3354/cr01378

30. Liesivaara P, Meuwissen M, Myyrä S. Government Spending under Alternative Yield Risk Management Schemes in Finland. Agricultural and Food Science. 2017; 26(4). https://doi.org/10.23986/afsci.65247

31. Survey UG. Landsat surface reflectance data. Reston, VA; 2015.

32. Masek JG, Vermote EF, Saleous NE, Wolfe R, Hall FG, Huemmrich KF, et al. A Landsat surface reflectance dataset for North America, 1990-2000. IEEE Geoscience and Remote Sensing Letters. 2006; 3 (1):68–72. https://doi.org/10.1109/LGRS.2005.857030

33. Foga S, Scaramuzza PL, Guo S, Zhu Z, Dilley RD, Beckmann T, et al. Cloud detection algorithm comparison and validation for operational Landsat data products. Remote Sensing of Environment. 2017; 194:379–390. https://doi.org/10.1016/j.rse.2017.03.026

34. Peltonen-Sainio P, Jauhiainen L. Lessons from the Past in Weather Variability: Sowing to Ripening Dynamics and Yield Penalties for Northern Agriculture from 1970 to 2012. Regional Environmental Change. 2014; 14(4):1505–1516. https://doi.org/10.1007/s10113-014-0594-z

35. Azur MJ, Stuart EA, Frangakis C, Leaf PJ. Multiple imputation by chained equations: what is it and how does it work? International journal of methods in psychiatric research. 2011; 20(1):40–49. https://doi.org/10.1002/mpr.329 PMID: 21499542

36. Pedregosa F, Varoquaux G, Gramfort A, Michel V, Thirion B, Grisel O, et al. Scikit-learn: machine learning in Python. Journal of Machine Learning Research. 2011; 12(85):2825–2830.

37. Bishop CM. Pattern Recognition and Machine Learning. Berlin, Heidelberg: Springer-Verlag; 2006.

38. Fawcett T. An introduction to ROC analysis. Pattern Recognition Letters. 2006; 27:861–874. https://doi.org/10.1016/j.patrec.2005.10.010

39. Youden WJ. Index for rating diagnostic tests. Cancer. 1950; 3(1):32–35. https://doi.org/10.1002/1097-0142(1950)3:1%3C32::AID-CNCR2820030106%3E3.0.CO;2-3 PMID: 15405679